Second-order Fermi Reacceleration Mechanisms and Large-Scale Synchrotron Radio Emission in Intracluster Bridges

Gianfranco Brunetti[1,*] and Franco Vazza[2,1,3,†]

[1]*INAF—Istituto di Radioastronomia, via P. Gobetti 101, 40129 Bologna, Italy*
[2]*Dipartimento di Fisica e Astronomia, Universitá di Bologna, Via Gobetti 93/2, 40121 Bologna, Italy*
[3]*University of Hamburg, Hamburger Sternwarte, Gojenbergsweg 112, 21029 Hamburg, Germany*

Radio observations at low frequencies with the low frequency array (LOFAR) start discovering gigantic radio bridges connecting pairs of massive galaxy clusters. These observations probe unexplored mechanisms of *in situ* particle acceleration that operate on volumes of several Mpc^3. Numerical simulations suggest that such bridges are dynamically complex and that weak shocks and super-Alfvénic turbulence can be driven across the entire volume of these regions. In this Letter, we explore, for the first time, the role of second-order Fermi mechanisms for the reacceleration of relativistic electrons interacting with turbulence in these peculiar regions. We assume the turbulent energy flux measured in simulations and adopt a scenario in which relativistic particles scatter with magnetic field lines diffusing in super-Alfvénic turbulence and magnetic fields are amplified by the same turbulence. We show that steep spectrum and volume filling synchrotron emission can be generated in the entire intracluster bridge region, thus providing a natural explanation for radio bridges. Consequently, radio observations have the potential to probe the dissipation of energy on scales larger than galaxy clusters and second-order Fermi mechanisms operating in physical regimes that are still poorly explored. This has a potential impact on several branches of astrophysics and cosmology.

Introduction.—Mpc-scale, steep-spectrum, diffuse radio emission from the intracluster medium (ICM) is observed in the form of giant radio halos and relics in dynamically active and massive galaxy clusters (see [1,2] for reviews). This suggests that part of the kinetic energy that is dissipated in the ICM during cluster-cluster mergers is channelled into the acceleration of relativistic particles and amplification of magnetic fields through a hierarchy of complex mechanisms that transfer energy from Mpc scales to small scales, and that presumably involve shocks and turbulence operating in a unique plasma regime [3–12].

More recently, observations of low frequencies with the low frequency array (LOFAR) have discovered diffuse radio emission from regions extending on even larger scales and that connect pairs of massive clusters in a premerger phase [13,14]. These observations prove that these regions, where the gas is likely compressed, are filled by relativistic electrons and magnetic fields that are generated on scales which had never been probed before. The most spectacular case is the 5 Mpc long radio bridge connecting the two massive clusters A399 and A401 [14], where the radio emission follows a filament of gas connecting the two clusters that was early discovered with the Planck satellite through the Sunyaev-Zeldovich effect [15].

What makes their interpretation challenging is that radio bridges appears as truly diffuse radio emissions on gigantic scales, suggesting that relativistic particles are accelerated *in situ* by mechanisms that are distributed on very large spatial scales and that are not necessarily powered by the energy dissipated as a consequence of major cluster-cluster mergers. While recent numerical simulations have suggested that *equatorial* shocks can be launched perpendicular to the merger axis even in a premerger phase [16], strong shocks are very rare in the hot and compressed gas of intracluster bridges [17]. For this reason the large area filling factor observed in the radio bridge of A399-A401 clearly disfavors shock acceleration as the main source of the observed emission and suggests that preexisting and volume filling suprathermal electrons are (re)accelerated to radio-bright energies ($> \mathrm{GeV}$) by other mechanisms. Numerical simulations show that relatively weak shocks, $\mathcal{M} \leq 2\text{–}3$, form in these regions and that up to $\sim 10\%$ of the volume has been crossed by these shocks in the last Gyr [14] leading to the possibility that radio bridges may result from reacceleration of a volume filling population of fossil relativistic electrons by these weak shocks under favorable projection effects. However, in order to match the constraints on the spectrum of the emission, this scenario requires assumptions on the age and dynamics of the fossil electrons that are not very plausible (see discussion in [14]). Virtually all major mergers should undergo a stage in which the remnant of a cosmic filament connecting the two clusters is compressed and preprocessed by gas dynamics, before the two clusters collide.

Therefore, recent detections [13,14] may have unveiled the tip of the iceberg of a common (albeit short-lived, i.e., ~Gyr) phenomenology. Understanding the mechanisms of acceleration of radio emitting particles in such pillars of the cosmic web is therefore also key to prepare to what the future generation of radio surveys will deliver [17]. In this Letter, we propose that fossil electrons, released in the ICM in the past by the activity of AGN and star-forming galaxies, are reaccelerated by the turbulence in the regions bridging massive premerging systems.

Dynamics and turbulence in bridges connecting clusters.—Massive binary mergers are rare and powerful events occurring in high over-density regions [18]. Even during its early stage, the dynamics of the collapse and the accretion of smaller subclusters drive weak shocks [16,17] and transonic turbulence [19]. We used cosmological MHD numerical simulations obtained with the ENZO code [20] to examine the properties of turbulence and magnetic fields in a binary cluster collision during its premerger phase. Specifically, we used the same pair of simulated clusters presented in [14,21] that closely resemble the A399-A401 pair, which is the reference of our work. Simulations have eight levels of adaptive mesh refinement (AMR) to selectively increase the spatial and force resolution down to $\Delta x = 3.95$ kpc/cell in most of the virial volumes of clusters, and assume a uniform primordial magnetic field $B_0 = 10^{-10}$ G (comoving) at the start of the simulation.

We attempt to separate turbulent fluctuations, δV, from bulk motions on larger scales using the filtering technique in [22] and extract solenoidal, $\nabla \cdot \vec{v} = 0$, and compressive, $\nabla \times \vec{v} = 0$, turbulent components using the Hodge-Helmholtz projection in Fourier space [22]. This allows us to estimate the local turbulent energy flux across scales, $F \sim 1/2\rho_{ICM}\delta V^3/L$, which is scale independent in Kolmogorv turbulence. We measure that ~60% of the turbulent energy flux in the bridge is associated to solenoidal motions. Figure 1 shows the projected energy flux of the solenoidal component measured when the two clusters are in a premerger stage ($z = 0.1$) in a situation (cluster masses and dynamics) similar to A399-A401. Turbulence in the bridge has injection scales $L \sim 400$ kpc–1 Mpc [see also 17] and is powered by the accretion of matter and smaller subclusters (visible in Fig. 1 and the Supplemental Material [23]) on the overdense region containing the two main clusters; the detection of x-ray bremsstrahlung from these subclusters and from the bridge itself is however challenging with present x-ray telescopes (see discussion in Sec. 3.3.4 of [17]). In particular, solenoidal motions originate from baroclinic instabilities at curved shocks and compressive amplification of accreted vortical motions [19,24,25], and from the generation of vorticity by shear stresses [22].

In the region connecting the clusters (a cylinder 1.5 Mpc × 3 Mpc, $V \sim 5$ Mpc³) we measure a turbulent luminosity $F \cdot V \sim 10^{45}$ erg s⁻¹ (masking regions around small subclusters where F can be biased high by our
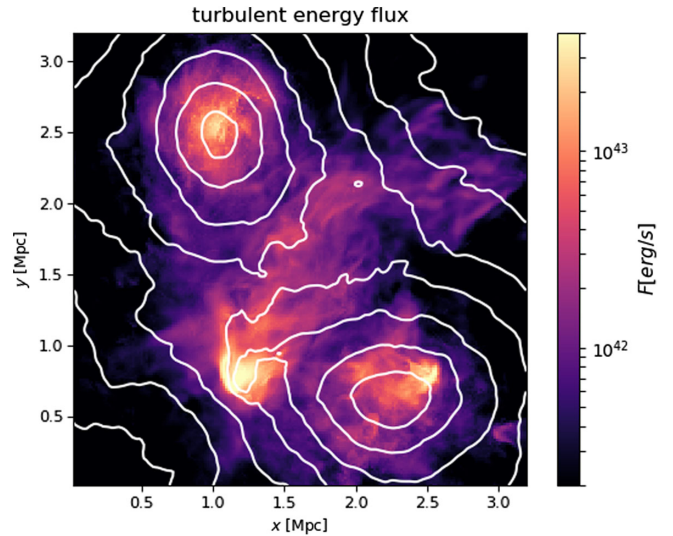

FIG. 1. Map of kinetic energy flux integrated along the line of sight (5.1 Mpc) for the simulated system at $z=0.1$, with logarithmically spaced gas projected density contours ($\Delta \log_{10} n = 0.25$).

filtering). This is similar to the luminosity found in simulated clusters during mergers [22,26]. Solenoidal turbulence is a key ingredient for magnetic field amplification in the ICM via small scale dynamo [11,12,24,27], which indeed is a mechanism that is observed in the central regions of clusters in MHD simulations [21,28–30]. However, in intracluster bridges this process is quenched by the limited spatial resolution in our simulations $\Delta x \gg l_A$; l_A being the MHD scale where the velocity of turbulent eddies equals the Alfvén speed and where most of the amplification takes place. We thus estimate the field in post processing [23]. The plasma in intracluster bridges shares conditions similar to the medium in the outskirts of galaxy clusters, being a weakly collisional and unstable high beta plasma with presumably very high effective Reynolds number [31–35]. Under these conditions, after the turbulent cascade reaches dissipation scales, a fixed fraction of the energy flux of MHD turbulence is channeled into magnetic field [36]. We thus estimate the magnetic field in our simulation as $B^2/8\pi \sim \eta_B F \tau_e \sim \frac{1}{2}\eta_B \rho_{ICM}\delta V^2$, where τ_e is the eddy turnover time $\tau_e \sim L/\delta V$, and $\eta_B \sim$ a few percent. We obtain a volume-averaged field in the bridge $\langle B \rangle \sim 0.5$–0.6 μG, that is ~3 times larger than the original field in our simulations. This is ~3–5 times smaller than the typical field in the internal regions of galaxy clusters [1,21] implying values of the beta plasma, $\beta_{pl} \sim 100$–200, which are slightly larger than those in clusters. This is because bridges are dynamically younger regions, and their lifetime 1–1.5 Gyr (collision time of clusters) is comparable to the turbulent eddy-turnover times, $\tau_e \sim 0.4$–1 Gyr, in these regions.

Turbulent reacceleration model.—Turbulent acceleration drains a fraction of the turbulent energy flux into particles:

$$\frac{\rho_{\mathrm{ICM}}\delta V^3}{L}\eta_{CRe} \sim \int d^3 p E \frac{\partial f_e}{\partial t} \qquad (1)$$

where η_{CRe} is the electron acceleration efficiency, the right term describes the energy flux into accelerated electrons, and f_e is the electrons distribution function in the momentum space. Radio emitting electrons in the ICM lose energy mainly through synchrotron emission and inverse Compton (IC) scattering off the cosmic microwave background (cmb) photons. The turbulent luminosity measured in the simulated bridge ($\approx 10^{45}$ erg s^{-1}) should be compared to the total (IC and synchrotron) nonthermal luminosity of the bridge, $L_{\mathrm{IC}+S} \sim L_S[1+(B_{\mathrm{cmb}}/B)^2]$, where $L_s \sim 10^{40}$ erg s^{-1} is the radio luminosity of A401-A399 [14] and $B_{\mathrm{cmb}} = 3.25(1+z)^2$ μG. If we assume the magnetic field derived in the previous Section, the turbulent luminosity is $\gg 1000$ times the total nonthermal luminosity from the bridge, and thus only a small fraction of the turbulent energy flux is required to maintain the nonthermal emission. Energetic particles in a turbulent medium can be subject to second-order Fermi acceleration. Several studies considered the transit time damping (TTD) with compressive modes in the ICM [4,5,37]. More recently, Brunetti and Lazarian [38] proposed a mechanism that operates in large-scale super-Alfvénic solenoidal turbulence in the ICM, where particles are reaccelerated, stochastically diffusing across regions of magnetic reconnection and dynamo (see [39,40] for the application to gamma-ray bursts and Pulsar wind nebulae). On much smaller scales, situations involving first-order and second-order Fermi-like acceleration are also observed in simulations of reconnection regions [41–44]. In the case of prevalence of solenoidal component and strongly super-Alfvénic turbulence, $M_A^2 = (\delta V/V_A)^2 \sim M^2\beta_{\mathrm{pl}} \gg 1$, as in the simulated bridges where $M_A \sim 8$–10 ($M_A \sim 30$ assuming the original field values from simulations), this acceleration mechanism may become faster than TTD [23]. Thus following [38] we adopt a diffusion coefficient in the particle momentum space (assuming a reference value for the effective mfp of relativistic electrons $\sim 1/2l_A$, [23]):

$$D_{pp} \sim \frac{48}{c}\frac{F}{\rho_{\mathrm{ICM}}V_A}p^2 \qquad (2)$$

By adopting our magnetic field model, the Alfvén speed is $V_A \simeq \sqrt{(2/\rho_{\mathrm{ICM}})(FL/\delta V)\eta_B}$ and $D_{pp} \propto p^2 \eta_B^{-1/2}\delta V^2/L$. We thus use Eq. (2) and the energy flux of the solenoidal turbulence measured in the simulated bridge to calculate the electrons reacceleration time $\tau_{\mathrm{acc}} = p^2/(4D_{pp})$. We calculate the acceleration time in 81 000 cells sampling the region connecting the two simulated clusters [23]. The results are shown in Fig. 2 for three values of η_B. The acceleration times are very long, as expected for second-order Fermi mechanisms, however they are much shorter than the dynamical timescale of bridges and the
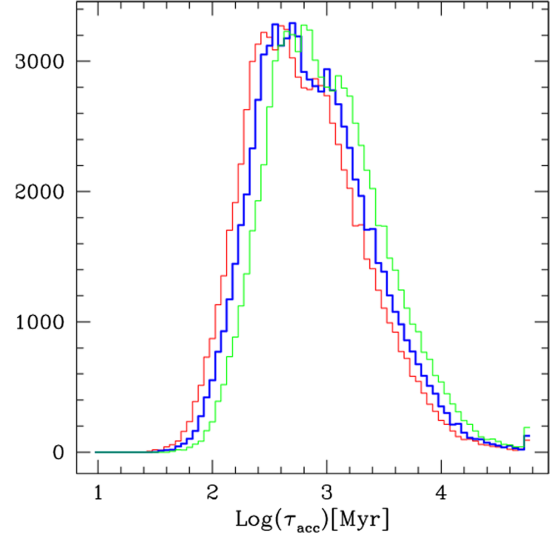

FIG. 2. Number of cells as a function of the particle acceleration time (81 000 cells sampling the simulated bridge) assuming $\eta_B = 0.02$ (red), 0.03 (blue), 0.05 (green).

turbulent eddy turnover times. Most important, in $\sim 1/3$–$1/2$ of the volume the acceleration time is similar to, or smaller than, the cooling time of radio emitting electrons at the redshift of the A399-A401 system, $\tau \sim 220(B_{\mu G}/0.5)^{1/2}(\nu_{\mathrm{MHz}}/150)^{-1/2}$ Myr (assuming $B_{\mathrm{cmb}}^2 \gg B^2$). This allows us to conclude that the mechanism can naturally generate volume filling synchrotron emission from the entire bridge.

Spectrum of the emission.—Next we evaluate whether the radio spectrum of the bridge in A399-A401 can be explained by our model. We calculate the evolution of the electrons distribution function, $N = 4\pi f p^2$, in the general situation in which relativistic electrons and protons, injected in the volume in the past by galaxies and AGN, coexist. We combine Fokker-Planck equations for primary and secondary electrons:

$$\begin{aligned}\frac{\partial N_e(p,t)}{\partial t} &= \frac{\partial}{\partial p}\left(N_e(p,t)\left[\mathcal{S}_e(p)-\frac{p}{3}(\nabla \cdot V)\right]\right)\\&+ \frac{\partial}{\partial p}\left(D_{pp}\frac{\partial N_e(p,t)}{\partial p}-\frac{2}{p}N_e(p,t)D_{pp}\right)\\&+ Q_e(p,t),\end{aligned} \qquad (3)$$

and protons

$$\begin{aligned}\frac{\partial N_p(p,t)}{\partial t} &= \frac{\partial}{\partial p}\left(N_p(p,t)\left[\mathcal{S}_p(p)-\frac{p}{3}(\nabla \cdot V)\right]\right)\\&+ \frac{\partial}{\partial p}\left(D_{pp}\frac{\partial N_p(p,t)}{\partial p}-\frac{2}{p}N_p(p,t)D_{pp}\right)\\&- \frac{N_p(p,t)}{\tau_{pp}}.\end{aligned} \qquad (4)$$
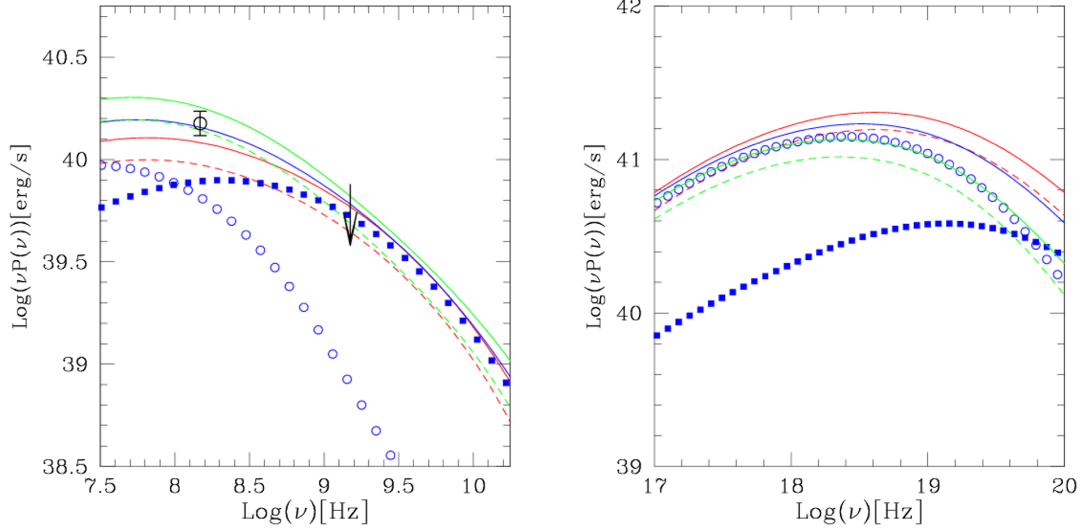
FIG. 3.   Synchrotron (left) and IC (right) spectra obtained for $\eta_B = 0.02$ (red), 0.03 (blue), and 0.05 (green). Dashed lines (for $\eta_B = 0.02$ and 0.05) mark models assuming only primary electrons. The contribution from regions with larger (85% of cells in the volume) and shorter acceleration times (15% of the volume) are also marked with open and filled points, respectively, considering $\eta_B = 0.03$. Radio data are taken from [14].

$\mathcal{S}$ accounts for the energy losses of electrons (Coulomb, ICS, and synchrotron) and protons (Coulomb), D_{pp} is given by Eq. (2), $\tau_{pp} = (n_{ICM}\sigma_{pp}c)^{-1}$ is the timescale of inelastic pp collisions in the ICM, Q_e is the injection spectrum of secondary electrons by pp collisions, and $\nabla \cdot V$ accounts for compression (e.g., for details, see [45]). In principle, the evolution of particles should be computed by following their spatial advection with a Lagrangian tracer approach [25] and then by integrating in time Eqs. (3) and (4) for each tracer [46]. However, this approach is numerically challenging and clearly beyond the exploratory goal of the present Letter. Here we adopt a simple *single zone* model, assuming average quantities that are measured in the simulated bridge region at a fixed time $z = 0.1$, namely $kT = 5$ keV, $n_{ICM} = 3 \times 10^{-4}$ cm^{-3} (both consistent with measurements in A399-A401), and $\nabla \cdot V \sim 0.75 \times 10^{-16}$ s^{-1}. We then assume different τ_{acc} spanning the range of values in Fig. 2 and for each value of τ_{acc} calculate electrons spectra from Eqs. (3) and (4) assuming $B = \langle B \rangle$ and evolving spectra for one turbulent eddy turnover time $\langle \tau_e \rangle$. Specifically, for each τ_{acc}, $\langle B \rangle$ and $\langle \tau_e \rangle$ are obtained by averaging the values of B and τ_e in the cells with acceleration time $= \tau_{acc}$. Finally, we obtain the emission integrated from the bridge region by combining the emissions generated by each electron spectrum weighted for the probability distribution function of the acceleration times at $z = 0.1$ (from Fig. 2). The remaining ingredient is the initial spectrum and number of the *seed* electrons and protons to reaccelerate. This is largely unknown in bridges and filaments connecting clusters. However, as in the case of clusters, we expect that seeds primary electrons injected by the past activity of shocks, AGN, and galactic winds, can be accumulated in the entire

region of the bridge at energies of ~100 MeV where their cooling time is maximised [2]. In Fig. 3 we show the synchrotron and IC spectra calculated assuming the volume of the radio bridge in A399-A401 $= 5$ Mpc^3 [14] for an initial spectrum of primary electrons and protons injected at $z = 0.2$ and passively evolved to $z = 0.07$; the final results are only little sensitive on the exact shape of the initial spectra as they evolve nonlinearly with time due to turbulent acceleration and losses. The initial energy densities of relativistic protons and primary electrons in Fig. 3 (solid lines) are assumed 10^{-2} and 3×10^{-5} of the thermal ICM; these are typical values assumed in radio halo models. In Fig. 3 we also show the case with only primary electrons (dashed lines), i.e., without including protons. Figure 3 shows that the synchrotron spectrum peaks at few hundred MHz, matching well the LOFAR detection [14], and extends to higher frequencies, where detections are still missing. The IC spectrum peaks in the hard x-rays with a luminosity ~10–20 times larger than the synchrotron luminosity. Spectra are sensitive to the turbulent energy flux measured in simulations and scale (linearly) with the amount of seed electrons to reaccelerate, whereas they are not very sensitive to η_B. The cutoff synchrotron frequency emitted by the reaccelerated electrons is $\nu_c \propto p_m^2 B$, where $p_m \sim 4D_{pp}/\mathcal{S}$ is the maximum momentum of electrons. In our model (for $B_{cmb}^2 \gg B^2$), this gives:

$$\nu_c \propto F^2 \rho_{ICM}^{-1} \epsilon_t^{-1} \eta_B^{-\frac{1}{2}}, \qquad (5)$$

where $\epsilon_t \sim 1/2\rho_{ICM}\delta V^2$. The cutoff synchrotron frequency depends on the turbulent energy flux and turbulent energy density. Consequently a natural prediction of our model is

that the synchrotron emission at lower frequencies should be more volume filling, while at higher frequencies it should be contributed by the most turbulent regions that fill a smaller fraction of the volume. This is indeed shown in Fig. 3 where we report the synchrotron and IC spectrum from cells with $\tau_{\rm acc} > \tau_*$ (filling 85% of the volume; empty circles) and with $\tau_{\rm acc} < \tau_*$ (15% of volume; filled squares); τ_* is a threshold value. Finally, we notice that weak shocks in the bridge [14] may also compress the population of turbulent reaccelerated electrons and the magnetic fields increasing the radio brightness at their location.

Conclusions.—In this Letter we propose that the radio bridges extending on scales larger than clusters originate from second-order Fermi acceleration of electrons interacting with turbulence. We show that the physical conditions and very long dynamical timescales in bridges connecting clusters allow the effects of these gentle mechanisms to become important. Turbulence is generated by the complex dynamics of substructures in bridges and thus, according to the proposed scenario, radio observations are also novel probes of the dynamics and dissipation of gravitational energy on very large scales. More specifically we extract the turbulent properties measured in cosmological simulations mimicking the A399-A401 system and assume a second-order Fermi mechanism from the interaction of relativistic particles with magnetic field lines diffusing in super-Alfvénic turbulence. We demonstrated that the mechanism allows for the reacceleration of radio emitting electrons in a large fraction of the volume. This can generate a volume-filling synchrotron emission with luminosities compatible with the observed ones and steep spectra, with $\alpha \sim 1.3$–1.5 between 0.15–1.5 GHz [$L(\nu) \propto \nu^{-\alpha}$] or steeper. The same turbulence amplifies magnetic fields in the bridge. This results in a field that is stronger than that obtained directly from current cosmological simulations, with a potential impact on studies based on Faraday rotation and on the propagation of very high energy cosmic rays. Future observations will test crucial predictions of the model: the filling factor of the radio emission should be larger at the low frequencies observable with LOFAR, making the emission smoother there, while it is predicted to decrease at higher frequencies, where the emission gets dominated by the clumpy contribution from smaller regions with high acceleration rate. Finally, our model predicts IC emission in the hard x-rays with a luminosity 10–30 times larger than the synchrotron component.

*brunetti@ira.inaf.it
†franco.vazza2@unibo.it

[1] R. J. van Weeren, F. de Gasperin, H. Akamatsu, M. Brüggen, L. Feretti, H. Kang, A. Stroe, and F. Zandanel, Space Sci. Rev. **215**, 16 (2019).

[2] G. Brunetti and T. W. Jones, Int. J. Mod. Phys. D **23**, 1430007 (2014).

[3] R. Cassano and G. Brunetti, Mon. Not. R. Astron. Soc. **357**, 1313 (2005).

[4] G. Brunetti and A. Lazarian, Mon. Not. R. Astron. Soc. **378**, 245 (2007).

[5] F. Miniati, Astrophys. J. **800**, 60 (2015).

[6] G. Brunetti, Plasma Phys. Controlled Fusion **58**, 014011 (2016).

[7] R. Xu, A. Spitkovsky, and D. Caprioli, arXiv:1908.07890.

[8] D. Ryu, H. Kang, and J.-H. Ha, Astrophys. J. **883**, 60 (2019).

[9] H. Kang and D. Ryu, Astrophys. J. **734**, 18 (2011).

[10] H. Kang, D. Ryu, and T. W. Jones, Astrophys. J. **756**, 97 (2012).

[11] D. Ryu, H. Kang, J. Cho, and S. Das, Science **320**, 909 (2008).

[12] F. Miniati and A. Beresnyak, Nature (London) **523**, 59 (2015).

[13] A. Botteon, T. W. Shimwell, A. Bonafede, D. Dallacasa, G. Brunetti, S. Mandal, R. J. van Weeren, M. Brüggen, R. Cassano, and F. de Gasperin, Mon. Not. R. Astron. Soc. **478**, 885 (2018).

[14] F. Govoni, E. Orrù, A. Bonafede, M. Iacobelli, R. Paladino, F. Vazza, M. Murgia, V. Vacca, G. Giovannini, and L. Feretti, Science **364**, 981 (2019).

[15] P. A. R. Ade *et al.* (Planck Collaboration), Astron. Astrophys. **550**, A134 (2013).

[16] J.-H. Ha, D. Ryu, and H. Kang, Astrophys. J. **857**, 26 (2018).

[17] F. Vazza, S. Ettori, M. Roncarelli, M. Angelinelli, M. Brüggen, and C. Gheller, Astron. Astrophys. **627**, A5 (2019).

[18] K. Roettiger, C. Loken, and J. O. Burns, Astrophys. J. Suppl. Ser. **109**, 307 (1997).

[19] L. Iapichino, W. Schmidt, J. C. Niemeyer, and J. Merklein, Mon. Not. R. Astron. Soc. **414**, 2297 (2011).

[20] G. L. Bryan *et al.* (Enzo Collaboration), Astrophys. J. Suppl. Ser. **211**, 19 (2014).

[21] P. Domínguez-Fernández, F. Vazza, M. Brüggen, and G. Brunetti, Mon. Not. R. Astron. Soc. **486**, 623 (2019).

[22] F. Vazza, T. W. Jones, M. Brüggen, G. Brunetti, C. Gheller, D. Porter, and D. Ryu, Mon. Not. R. Astron. Soc. **464**, 210 (2017).

[23] See the Supplemental Material at http://link.aps.org/supplemental/10.1103/PhysRevLett.124.051101 for additional figures showing the turbulent energy flux and the regions used to extract turbulent quantities. It also includes a more detailed discussion on the magnetic field model and on the comparison between the acceleration model used in the paper and the transit time damping mechanism.

[24] D. H. Porter, T. W. Jones, and D. Ryu, Astrophys. J. **810**, 93 (2015).

[25] D. Wittor, T. Jones, F. Vazza, and M. Brüggen, Mon. Not. R. Astron. Soc. **471**, 3212 (2017).

[26] S. Planelles and V. Quilis, Mon. Not. R. Astron. Soc. **399**, 410 (2009).

[27] K. Dolag, D. Grasso, V. Springel, and I. Tkachev, J. Cosmol. Astropart. Phys. 01 (2005) 009.

[28] J. A. ZuHone, M. Markevitch, and D. Lee, Astrophys. J. **743**, 16 (2011).

[29] F. Vazza, G. Brunetti, M. Brüggen, and A. Bonafede, Mon. Not. R. Astron. Soc. **474**, 1672 (2018).

[30] J. Donnert, F. Vazza, M. Brüggen, and J. ZuHone, Space Sci. Rev. **214**, 122 (2018).

[31] A. A. Schekochihin and S. C. Cowley, Phys. Plasmas **13**, 056501 (2006).

[32] A. Lazarian and A. Beresnyak, Mon. Not. R. Astron. Soc. **373**, 1195 (2006).

[33] A. A. Schekochihin, S. C. Cowley, F. Rincon, and M. S. Rosin, Mon. Not. R. Astron. Soc. **405**, 291 (2010).

[34] G. Brunetti and A. Lazarian, Mon. Not. R. Astron. Soc. **412**, 817 (2011).

[35] R. Santos-Lima, E. M. de Gouveia Dal Pino, G. Kowal, D. Falceta-Gonçalves, A. Lazarian, and M. S. Nakwacki, Astrophys. J. **781**, 84 (2014).

[36] A. Beresnyak, Phys. Rev. Lett. **108**, 035002 (2012).

[37] A. Pinzke, S. P. Oh, and C. Pfrommer, Mon. Not. R. Astron. Soc. **465**, 4800 (2017).

[38] G. Brunetti and A. Lazarian, Mon. Not. R. Astron. Soc. **458**, 2584 (2016).

[39] S. Xu and B. Zhang, Astrophys. J. Lett. **846**, L28 (2017).

[40] S. Xu, N. Klingler, O. Kargaltsev, and B. Zhang, Astrophys. J. **872**, 10 (2019).

[41] G. Kowal, E. M. de Gouveia Dal Pino, and A. Lazarian, Phys. Rev. Lett. **108**, 241102 (2012).

[42] J. T. Dahlin, J. F. Drake, and M. Swisdak, Phys. Plasmas **21**, 092304 (2014).

[43] F. Guo, X. Li, W. Daughton, P. Kilian, H. Li, Y.-H. Liu, W. Yan, and D. Ma, Astrophys. J. Lett. **879**, L23 (2019).

[44] L. Comisso and L. Sironi, Astrophys. J. **886**, 122 (2019).

[45] G. Brunetti, S. Zimmer, and F. Zandanel, Mon. Not. R. Astron. Soc. **472**, 1506 (2017).

[46] J. Donnert and G. Brunetti, Mon. Not. R. Astron. Soc. **443**, 3564 (2014).